21

High-Resolution Imaging of Bacteriorhodopsin by Atomic Force Microscopy

Dimitrios Fotiadis and Andreas Engel

1. Introduction

In the last years the atomic force microscope (AFM; **ref. *1***) has become a powerful imaging tool for the biologist. The unique features like the possibility to image biological structures in their native environment (i.e., in buffer solution, at room temperature, and under normal pressure), the high lateral and vertical resolution, and the high signal-to-noise ratio of the topographs acquired by AFM make this instrument outstanding. It has made the observation of different single biomolecules at work and the monitoring of biomolecular interactions by time-lapse AFM possible (for recent reviews, *see* **refs. *2–4***).

This chapter focuses on the application of contact mode AFM to acquire high-resolution structural information of membrane proteins in buffer solution. In this scan mode the probing tip touches the surface with a constant force while scanning. To minimize possible damage of the biological specimen by the tip, soft cantilevers with spring constants around 0.1 N/m must be used and scanning must be performed at minimal tip force (approx 100–300 pN). Lateral resolutions down to 0.41 nm and vertical resolutions down to 0.10 nm have been achieved on biological membranes in solution ***(5)***. Alternative AFM modes to record topographies are the tapping mode ***(6–8)*** and the magnetically activated oscillating mode ***(9,10)***, better known as MAC mode. Both are similar and frequently used to image the surface topography of weakly immobilized biomolecules, that is, single proteins, fibrils, and chromosomes, and have in common that the AFM tip is oscillated vertically while scanning the sample. Thus, frictional forces are reduced by the oscillation of the tip avoiding deformation and displacement of the sample. However, for high-resolution imaging of biological membranes contact mode has shown to be the better choice pro-

From: *Methods in Molecular Biology, vol. 242: Atomic Force Microscopy: Biomedical Methods and Applications*
Edited by: P. C. Braga and D. Ricci © Humana Press Inc., Totowa, NJ

vided the imaging parameters, for example, force and imaging buffer, are adjusted correctly ***(11)***. To prevent deformation of the structure as a result of friction, the forces acting between tip and sample should not exceed 300 pN in contact mode. However, application of higher forces can sometimes be useful to perform precise and controlled dissections of biological samples by manipulation with the AFM tip ***(12)***.

As biological specimen for the AFM imaging experiment presented here, we have chosen bacteriorhodopsin (BR) membranes. This 26-kDa heptahelical transmembrane protein acts as a light-driven proton pump in the cell membrane of the bacterium *Halobacterium salinarum* ***(13,14)***. Photoisomerization of the covalently bound chromophore from all-*trans* to 13-*cis* retinal initiates proton translocation across the cell membrane ***(15,16)***. This establishes a proton gradient across the cell membrane for ATP synthesis and other energy requiring processes in the cell. BR molecules form highly ordered two-dimensional crystals ***(17)*** (trigonal lattice: $a = b = 6.2$ nm, $\gamma = 60°$) in the native membrane of *Halobacterium salinarum*, termed purple membrane for its color. Because of its crystallinity and flatness this sample is very suitable for AFM and cryo-electron microscopy. High-resolution three-dimensional structures of BR (**Fig. 1**) were determined by electron crystallography and X-ray diffraction (for a recent review, *see* **ref. *18***). In BR, the retinal (*see* **Fig. 1**; arrowhead) lies in the intramembrane cavity formed by the seven transmembrane α-helices generally denoted A to G. The main portions of BR that protrude out of the membrane are: The loops connecting the transmembrane α-helices A and B as well as E and F (AB and EF loops; **Fig. 1**) on the cytoplasmic side and the B-C interhelical loop (BC loop; **Fig. 1**) on the extracellular side. The latter forms a twisted antiparallel β-sheet and is more stable than the wobbly EF loop ***(19)***.

2. Materials

2.1. Preparation of Mica Supports for Sample Immobilization

1. Inoxydable and magnetic steel disks of 11 mm in diameter (internal services of the Biozentrum, Basel, Switzerland).
2. Teflon sheets of 0.25-mm thickness (Maag Technic AG, Birsfelden, Switzerland).
3. Mica sheets with a thickness between 0.3–0.6 mm (Mica House, 2A Pretoria Street, Calcutta 700 071, India).
4. "Punch and die" set from Precision Brand Products Inc. (Downers Grove, IL).
5. Ethanol (concentration 96% [v/v]).
6. Loctite 406 superglue from KVT König, Dietikon, Switzerland.
7. Araldit Rapid: Two-component epoxy glue from Ciba-Geigy, Basel, Switzerland.
8. Scotch tape.

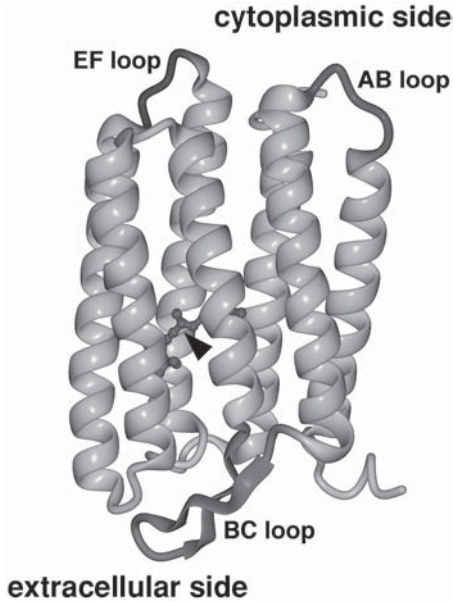

Fig. 1. Ribbon diagram of BR. The retinal chromophore (arrowhead) is displayed as a ball-and-stick model. This illustration of BR was calculated using the coordinates of Kimura et al. ***(28)*** and the three-dimensional visualization program DINO (http://www.dino3d.org/).

2.2. BR and Buffers (see *Note 1)*

1. Purple membranes of *H. salinarum*. Stock solution: 0.25 mg/mL in double distilled water containing 0.01% NaN_3. Store at 4°C and protect from unnecessary light irradiation.
2. Adsorption buffer: 20 m*M* Tris-HCl, pH 7.8, 150 m*M* KCl.
3. Imaging buffer for the extracellular side (ES imaging buffer): 20 m*M* Tris-HCl, pH 7.8, 150 m*M* KCl, 25 m*M* $MgCl_2$.
4. Imaging buffer for the cytoplasmic side (CS-imaging buffer): 20 m*M* Tris-HCl, pH 7.8, 150 m*M* KCl.

2.3. AFM and Accessories (see *Note 2)*

1. A commercial multimode AFM equipped with a 120-µm scanner (j-scanner) and a liquid cell (Digital Instruments, Veeco Metrology Group, Santa Barbara, CA).
2. Oxide-sharpened Si_3N_4 micro cantilevers of 100 µm in length and a nominal spring constant of k = 0.08 N/m (Olympus Optical Co., LTD, Tokyo, Japan).

3. Method

3.1. Preparation of Mica Supports for Sample Immobilization

1. Punch mica disks of 6 mm and Teflon disks of 13 mm diameter using the "punch and die" set and a hammer.
2. Clean the Teflon and steel disks with ethanol and paper wipes.
3. Glue a Teflon disk on a steel disk using Loctite 406.
4. Glue a mica disk on the Teflon surface of the Teflon-steel disk with the two-component epoxy glue.
5. Let the supports dry for at least 1 day.

3.2. Adsorption of BR to Mica

1. Dilute and mix 3 μL of purple membrane stock solution with 30 μL of adsorption buffer in an Eppendorf tube.
2. Cleave mica with Scotch tape.
3. Pipet the diluted purple membranes on the freshly cleaved mica support.
4. Adsorb BR for 15 to 30 min.
5. Wash away the purple membranes that are not firmly attached to the mica by removing approximately two thirds of the fluid volume from the mica surface and readding the same amount of the corresponding imaging buffer. Repeat this washing procedure at least three times.
6. Transport the support onto the piezo scanner.
7. Mount the AFM head containing fluid cell (without o-ring seal) and cantilever on the microscope.
8. Fill the space between the mica surface and the fluid cell with the corresponding imaging buffer to avoid drying of the protein.

3.3. Operation of the AFM (see Notes 3–5)

After thermal relaxation of the instrument, initial engagement of the tip is performed. Specimen deformation and contamination of the tip is minimized during the engagement process by setting the scan size to 0. Prior scanning the surface, the operating point of the instrument is set to forces below 1 nN. During scanning the forces are kept as small as possible (<300 pN) and corrected manually to compensate for thermal drift.

Two frames of 512 by 512 pixel are simultaneously recorded either showing topography or deflection signal in trace or retrace direction. Usually deflection and height signals are recorded at low magnification (frame size >1 μm) whereas height signals were acquired in both, trace and retrace direction at high magnification (frame size <1 μm).

This allows deformation of the sample in the fast scan direction to be detected and to be minimized by lowering the force applied to the stylus. Typically, the scan speed is set to 4.7–5.5 Hz (lines per second). At high magnification the scan range of the z piezo is reduced to avoid limitation of the axial

z-resolution by the digitalization of the signal (AD conversion). All measurements are carried out under ambient pressure and at room temperature.

3.4. Conclusion

Here we have presented materials and methods to image the native surface of bacteriorhodopsin at subnanometer resolution with the AFM in buffer solution (*see* **Note 6**). We have demonstrated that forces between stylus and sample as well as shape and geometry of the AFM tip play an important role for successful imaging of the biological sample (*see* **Note 7**). Additionally, it was shown that higher forces may be of advantage to study otherwise hidden features of a protein, that is, the AB loop in BR (*see* **Note 5**).

4. Notes

1. Buffer conditions for high-resolution AFM imaging: Topographs of native membrane proteins with a lateral resolution of 0.41 nm ***(5)*** can reproducibly be recorded with the AFM provided imaging force and buffer are adjusted correctly ***(11)***. In general, scanning is performed at minimal forces applied to the stylus to avoid friction and deformation of the biological sample. However, often even the smallest force adjustable by the instrument is too high for preventing deformation of the biomolecule.
   The effective interaction force acting between AFM stylus and specimen is the sum of the force applied to the stylus, the electrostatic repulsion and the van der Waals attraction between the two surfaces. By adjusting pH and ion strength of the imaging buffer van der Waals attraction and electrostatic repulsion between tip and sample can be balanced. Under these conditions the tip is assumed to surf on a cushion of electrostatic repulsion minimizing the deformation of the biomolecule. The best imaging conditions are determined by recording and analyzing force-distance curves between tip and sample in different buffers. Conditions that yield force curves with a small repulsive peak are ideal for high-resolution imaging. By this screening method the two slightly different imaging buffers for BR mentioned in **Subheading 2.2.** (CS and ES imaging buffer) were found. For further reading on this topic, *see* **ref. *11***.
2. Damping of vibrations: For high-resolution AFM imaging, an acoustic and vibration isolated set-up of the microscope is crucial. Antivibration and damping tables, or lead platforms supported by bungees offer excellent vibration damping. Acoustic isolation of the AFM can efficiently be achieved by a vacuum bell jar.
3. Morphology of BR crystals. **Figure 2** shows a typical overview (frame size 25 μm) of purple membranes adsorbed to freshly cleaved mica. The diameter of the BR sheets varies between 0.5–1.5 μm. The number of adsorbed membrane patches depends on the adsorption buffer, time and the concentration of the bacteriorhodopsin solution deposited on the mica. To avoid contamination of the tip, BR sheets were not adsorbed too densely on the support. At higher magnification (**Fig. 3**; frame size 3.67 μm) two different types of membranes can be

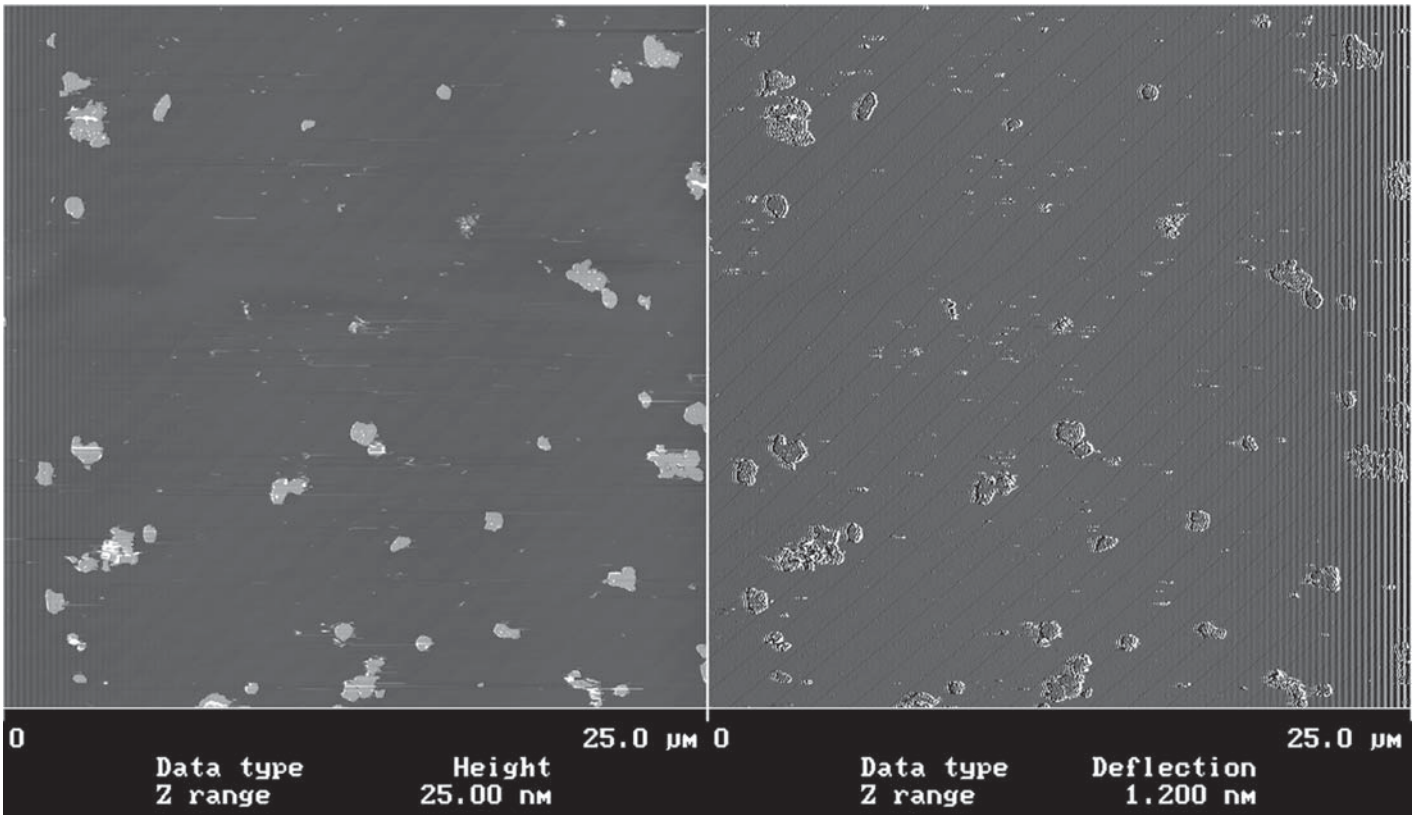

Fig. 2. Low-magnification AFM topograph (left) and deflection image (right) of purple membranes adsorbed to mica. The average height of the membranes was approx 6 nm under the given buffer conditions. Imaging buffer: 20 m*M* Tris-HCl, pH 7.8, 150 m*M* KCl.

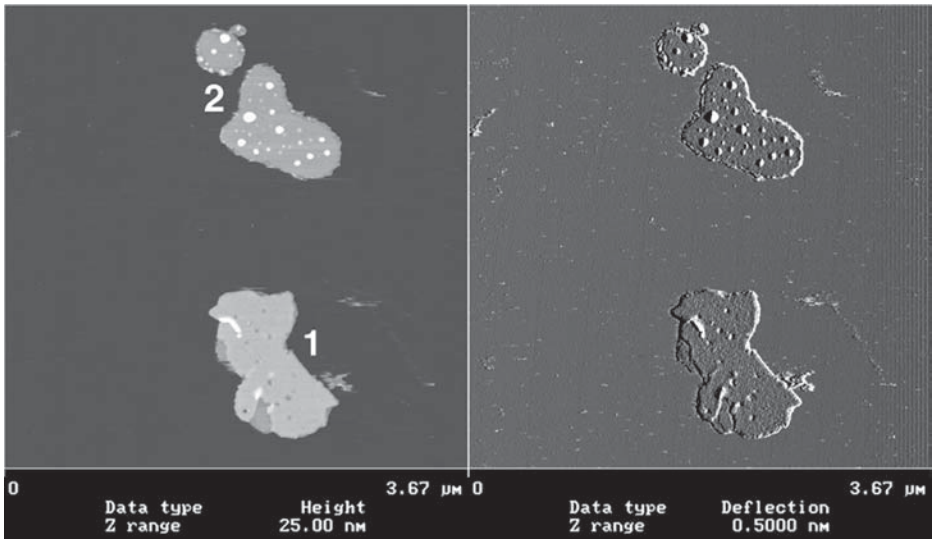

Fig. 3. Medium magnification AFM topograph (left) and deflection image (right) of two purple membranes exposing the extracellular (1) and the cytoplasmic (2) side. Imaging buffer: 20 m*M* Tris-HCl, pH 7.8, 150 m*M* KCl.

discerned. The extracellular side is characterized by small holes (**Fig. 3**, 1), whereas the cytoplasmic side by protruding bumps (**Fig. 3**, 2; **refs. *20*** and ***21***). A further feature that can be used to discriminate between the two sides is the small difference in thickness seen when scanning in CS imaging buffer. Purple membranes exposing the cytoplasmic side appear slightly lower than those exposing the extracellular one. As described by Müller et al. ***(22)*** ionic strength and pH affect the height measured between biological samples with different surface properties and their support.

4. The extracellular surface of BR: At high magnification the extracellular side of BR is characterized by protrusions extending 0.5 ± 0.1 nm out of the lipid bilayer (**Fig. 4**). The β-sheet in the loop connecting the transmembrane α-helices B and C constitutes the main part of the observed protrusion. For clarity a part of the image (17 nm × 17 nm frame) around the contoured trimer in **Fig. 4** was extracted and enlarged (see inset). An estimate of the resolution of this topograph is given below in **Subheading 4.6.**
5. The cytoplasmic surface of BR: Force-induced conformational changes: Imaging of the cytoplasmic surface is force-dependent because of the flexible EF loop ***(23,24)***. At approx 100 pN applied to the AFM stylus (**Fig. 5**; areas 1 and area in the inset above the broken line) the fully extended EF loops can be discerned as sharp protrusions of 0.8 ± 0.2 nm height. These become less prominent if the loading force is increased to approx 300 pN (**Fig. 5**; area 2 and area in the inset

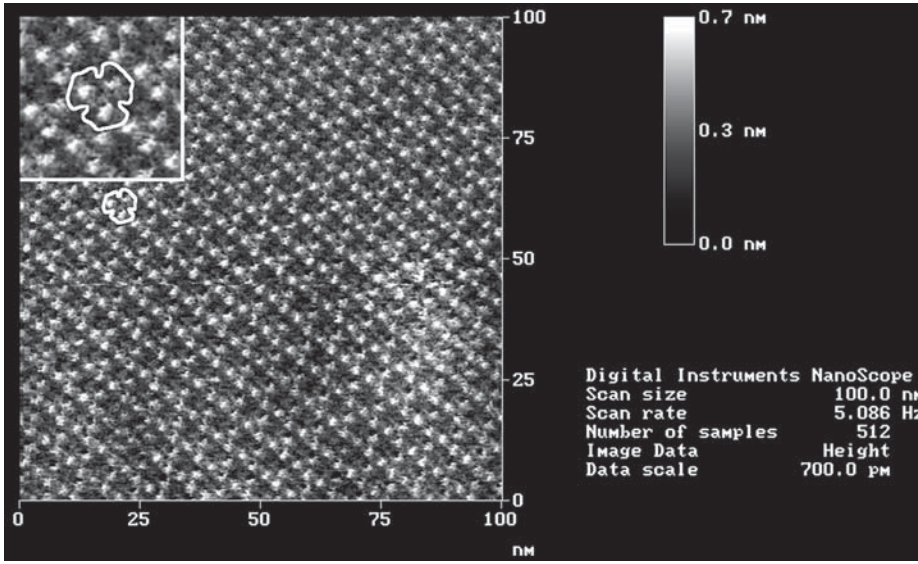

Fig. 4. High-magnification AFM topograph of the extracellular side of BR. For clarity, the square area (17 × 17 nm) around the contoured BR trimer was enlarged and is displayed in the inset. Imaging buffer: 20 m*M* Tris-HCl, pH 7.8, 150 m*M* KCl, 25 m*M* $MgCl_2$.

below the broken line). In the contoured trimer (inset) the two different states can clearly be seen: The upper two EF-loops are fully extended (above the broken line: applied force approx 100 pN) whereas the third one (below the broken line: applied force approx 300 pN) is pushed away by the tip and is therefore less prominent. Instead, the AB loops become visible at approx 300 pN applied to the AFM tip with a height of 0.6 ± 0.1 nm above the lipid bilayer. The advantage of such force induced conformational changes is that shorter loops covered by the bigger ones can be studied. If the applied force is further increased to approx 400 pN (**Fig. 5**; area 3) the BR trimers are hardly visible and horizontal streaks appear, indicating that the force is too high. When scanning at such high forces, care has to be taken because irreversible damages of the membrane may happen.

6. Estimating the resolution of AFM topographs: The resolution of a topograph containing a regular structure can be estimated from its powerspectrum. In the software package delivered with the AFM by Digital Instruments the option to calculate powerspectra of topographs is available. Otherwise various public domain programs like NIH image from the National Institutes of Health (Bethesda, MD) or SXM from the University of Liverpool (Liverpool, UK) have such algorithms implemented and can be downloaded for free (NIH image: http://rsb.info.nih.gov/nih-image/ and SXM: http://reg.ssci.liv.ac.uk/).

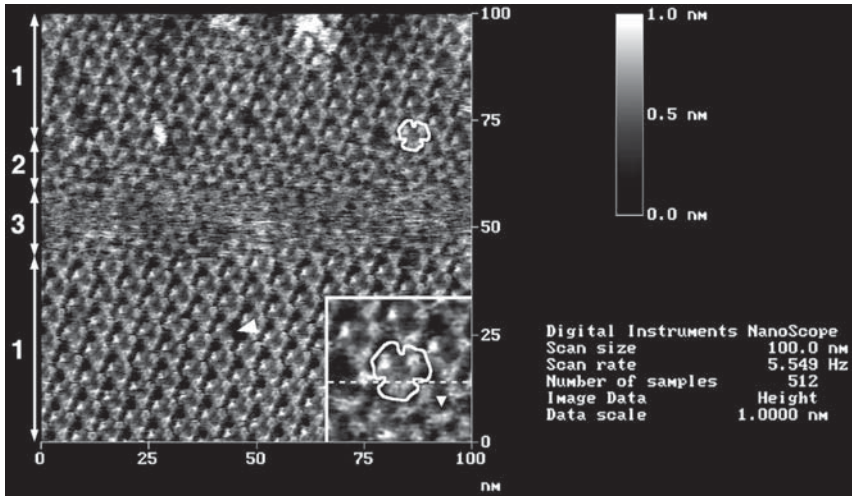

Fig. 5. Force-dependent AFM topography of the cytoplasmic side of purple membrane. At approx 100 pN (area 1) the EF loop is fully extended whereas at approx 300 pN (area 2) the loop is pushed away by the tip and is therefore not visible anymore. At approx 400 pN the BR trimers are hardly visible and streaks in the fast scan direction arise. This indicates that the applied force is too high and that irreversible damages may be inflicted to the membrane. For clarity, the square area (17×17 nm) around the contoured BR trimer was enlarged and is displayed in the inset. The broken line in the inset marks the force change from approx 100 to 300 pN. There, the contoured BR trimer contains both states of the EF loop: Two fully extended (above the broken line) and one where the loop was pushed away by the stylus (below the broken line). The triangle in the inset marks the threefold symmetry axis of a BR trimer recorded at approx 300 pN. Sometimes defective BR trimers with a monomer missing can be found (arrowhead). Imaging buffer: 20 m*M* Tris-HCl, pH 7.8, 150 m*M* KCl.

The calculated powerspectrum of the extracellular side (**Fig. 4**) is shown in **Fig. 6**. Diffraction patterns of this side of BR typically exhibit strong second order spots. The higher the order of the discernible spots, the higher is the resolution of the details preserved in the topograph. Here, sharp spots extend beyond the 1 nm resolution limit (see broken circle). The encircled spot (4,4) corresponds to a lateral resolution of 0.78 nm. To calculate the resolution at a selected diffraction spot (h,k) of such a trigonal lattice with lattice parameters: $a = b = 6.2$ nm and $\gamma = 60°$, Eq. (1) can be used. This formula is applicable to all lattice types, e.g., for orthorhombic lattices which also occur frequently in native and reconstituted two-dimensional crystals of membrane proteins (for further reading on crystallography, *see* **ref. *25***).

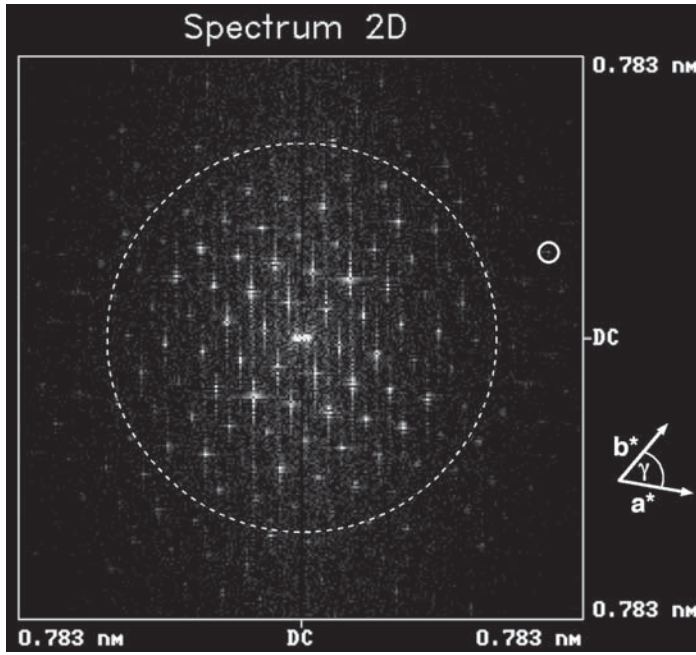

Fig. 6. Powerspectrum of the extracellular side of BR calculated from **Fig. 4**. Diffraction spot (4,4) represents a resolution of 0.78 nm (small circle). The broken circle represents the 1 nm resolution limit.

$$\delta = \frac{1}{|\vec{r}|} = \frac{\sin\gamma}{\sqrt{\frac{h^2}{a^2} + \frac{2 \cdot h \cdot k \cdot \cos\gamma}{a \cdot b} + \frac{k^2}{b^2}}}$$

where δ = resolution; a and b = basic lattice vectors; γ = angle between the basic lattice vectors; h and k = Miller indices; $\vec{r}$ = vector from origin to diffraction spot (h,k).

7. Tip effects and artifacts: At this time no commercial AFM tips are available with ideal point probes and perfect geometries in the subnanometer range. Therefore, tip effects and artifacts arising from the tip geometry are unavoidable and have to be considered when interpreting AFM topographies (for further reading on tip effects and artifacts, *see* **refs. *26*** and ***27***). Tip effects result when the probe interacts with the sample at different sites simultaneously, instead of at only one site. This leads to an AFM image of the sample features convoluted with the tip shape. To be sure of having acquired the correct surface structure and not an artifact, the same surface topography of the object being investigated has to be reproduced several times with different tips, from different batches. Tip artifacts can also be identified by changing the direction in which the AFM tip scans the sample (scan angle) because artifacts will rotate correspondingly ***(26)***. In addition, structures

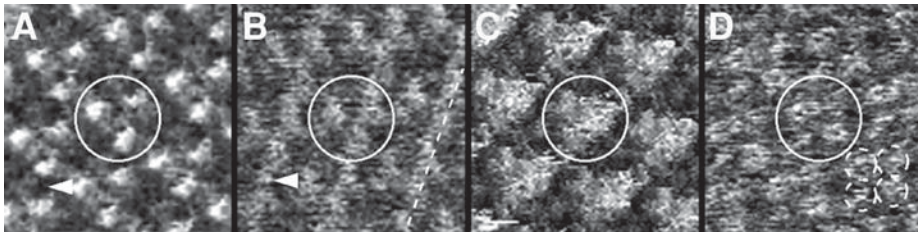

Fig. 7. Tip effects and artifacts. **A,** Artifact-free topography of the extracellular side of BR. **B** through **D,** Artifacteous topographies of the extracellular surface of BR. In all images the central trimers are encircled. In **A** (arrowhead) the lipid moiety separating the trimers is visualized whereas in **B** (arrowhead) not. The characteristic central depression in the BR trimer is completely missing in **C**. The broken circles in **D** mark four different protrusions instead of the three expected. The frame sizes in **A** to **D** are 17 nm. The heights are 0.7 nm **(A)**, 0.8 nm **(B)**, 1.2 nm **(C)**, and 0.7 nm **(D)**.

of samples that have been determined by other methods, for example, electron and X-ray crystallography for BR, can be used to further compare and confirm the observed AFM surface. The extracellular surface of BR recorded with an artifact-free tip is shown in **Fig. 7A** whereas **Fig. 7B** through **D** display images acquired with artifacteous tips. Tentative explanations of the observed artifacts are omitted because the statements would be too speculative. We restrict ourselves to a comparison of the artifacteous surfaces with the nonartifacteous one. Compared with **Fig. 7A**, the trimer in **Fig. 7B** has more the shape of an isosceles than an equilateral triangle indicating a distortion of the BR trimer. The lipid moiety that separates the neighboring trimers could not be visualized by the artifacteous tip (compare the areas marked by arrowheads in **Fig. 7A** and **B**). Along the broken line in **Fig. 7B** alternating heights between the prominent extracellular protrusions and the lipid moieties would be expected, but instead a rim of constant height is seen. In **Fig. 7C**, the depression at the threefold symmetry axis of the BR trimer is completely missing and the trimer seems to consist of a single plateau. The encircled BR trimer in **Fig. 7D** has lost its trigonal shape and resembles more a tetramer (the four protrusions constituting the tetramer are marked by broken circles). It should be noted that not the resolution of a topograph alone can be a figure of quality, but the crystallographic symmetry and the reproducibility must be considered as well.

Acknowledgments

This work was supported by the M. E. Müller-Foundation of Switzerland, the European Union-Quality of Life and Management of Living Resources Project (grant QLRT-2000-00778) and the Swiss National Center of Competence in Research "Nanoscale Science". The authors are indebted to Dr. Ansgar Philippsen for **Fig. 1**, to Dr. Patrick L. T. M. Frederix for fruitful discussions

and constructive comments on the manuscript and to Profs. Dieter Oesterhelt (Max-Planck-Institut für Biochemie, Martinsried, Germany) and Georg Büldt (Forschungszentrum Jülich, Jülich, Germany) for kindly providing us with BR.

References

1. Binnig, G., Quate, C. F., and Gerber, C. (1986) Atomic force microscope. *Phys. Rev. Lett.* **56,** 930–933.
2. Engel, A., Lyubchenko, Y., and Müller, D. J. (1999) Atomic force microscopy: A powerful tool to observe biomolecules at work. *Trends Cell Biol.* **9,** 77–80.
3. Stolz, M., Stoffler, D., Aebi, U., and Goldsbury, C. (2000) Monitoring biomolecular interactions by time-lapse atomic force microscopy. *J. Struct. Biol.* **131,** 171–180.
4. Engel, A. and Müller, D. J. (2000) Observing single biomolecules at work with the atomic force microscope. *Nat. Struct. Biol.* **7,** 715–718.
5. Stahlberg, H., Fotiadis, D., Scheuring, S., Rémigy, H., Braun, T., Mitsuoka, K., et al. (2001) Two-dimensional crystals: A powerful approach to assess structure, function and dynamics of membrane proteins. *FEBS Lett.* **504,** 166–172.
6. Zhong, Q., Inniss, D., Kjoller, K., and Elings, V. B. (1993) Fractured polymer/silica fiber surface studied by tapping mode atomic force microscopy. *Surf. Sci. Lett.* **290,** L688–L692.
7. Putman, C. A. J., Vanderwerf, K. O., de Grooth, B. G., Vanhulst, N. F., and Greve, J. (1994) Tapping mode atomic-force microscopy in liquid. *Appl. Phys. Lett.* **64,** 2454–2456.
8. Hansma, P. K., Cleveland, J. P., Radmacher, M., Walters, D. A., Hillner, P. E., Bezanilla, M., et al. (1994) Tapping mode atomic force microscopy in liquids. *Appl. Phys. Lett.* **64,** 1738–1740.
9. Han, W. H., Lindsay, S. M., and Jing, T. W. (1996) A magnetically driven oscillating probe microscope for operation in liquids. *Appl. Phys. Lett.* **69,** 4111–4113.
10. Han, W. H., Lindsay, S. M., Dlakic, M., and Harrington, R. E. (1997) Kinked DNA. *Nature* **386,** 563.
11. Müller, D. J., Fotiadis, D., Scheuring, S., Müller, S. A., and Engel, A. (1999) Electrostatically balanced subnanometer imaging of biological specimens by atomic force microscope. *Biophys. J.* **76,** 1101–1111.
12. Fotiadis, D., Scheuring, S., Müller, S. A., Engel, A., and Müller, D. J. (2002) Imaging and manipulation of biological structures with the AFM. *Micron* **33,** 385–397.
13. Oesterhelt, D. and Stoeckenius, W. (1973) Functions of a new photoreceptor membrane. *Proc. Natl Acad. Sci. USA* **70,** 2853–2857.
14. Oesterhelt, D. and Stoeckenius, W. (1971) Rhodopsin-like protein from the purple membrane of *Halobacterium halobium*. *Nat. New Biol.* **233,** 149–152.
15. Lanyi, J. K. (1993) Proton translocation mechanism and energetics in the light-driven pump bacteriorhodopsin. *Biochim. Biophys. Acta* **1183,** 241–261.
16. Khorana, H. G. (1988) Bacteriorhodopsin, a membrane protein that uses light to translocate protons. *J. Biol. Chem.* **263,** 7439–7442.

17. Blaurock, A. E. and Stoeckenius, W. (1971) Structure of the purple membrane. *Nat. New Biol.* **233,** 152–155.
18. Lanyi, J. K. and Luecke, H. (2001) Bacteriorhodopsin. *Curr. Opin. Struct. Biol.* **11,** 415–419.
19. Heymann, J. B., Müller, D. J., Landau, E. M., Rosenbusch, J. P., Pebay-Peyroula, E., Büldt, G., et al. (1999) Charting the surfaces of the purple membrane. *J. Struct. Biol.* **128,** 243–249.
20. Müller, D. J., Schoenenberger, C.-A., Büldt, G., and Engel, A. (1996) Immuno-atomic force microscopy of purple membrane. *Biophys. J.* **70,** 1796–1802.
21. Müller, D. J., Schabert, F. A., Büldt, G., and Engel, A. (1995) Imaging purple membranes in aqueous solutions at sub-nanometer resolution by atomic force microscopy. *Biophys. J.* **68,** 1681–1686.
22. Müller, D. J. and Engel, A. (1997) The height of biomolecules measured with the atomic force microscope depends on electrostatic interactions. *Biophys. J.* **73,** 1633–1644.
23. Müller, D. J., Sass, H.-J., Müller, S. A., Büldt, G., and Engel, A. (1999) Surface structures of native bacteriorhodopsin depend on the molecular packing arrangement in the membrane. *J. Mol. Biol.* **285,** 1903–1909.
24. Müller, D. J., Büldt, G., and Engel, A. (1995) Force-induced conformational change of bacteriorhodopsin. *J. Mol. Biol.* **249,** 239–243.
25. Misell, D. L. and Brown, E. B. (1987) Electron diffraction: An introduction for biologists, in *Practical Methods in Electron Microscopy*, vol. 12 (Glauert, A. M., ed.) Elsevier Science Publishers B. V., The Netherlands.
26. Xu, S. and Arnsdorf, M. F. (1994) Calibration of the scanning (atomic) force microscope with gold particles. *J. Microsc.* **173,** 199–210.
27. Schwarz, U. D., Haefke, H., Reimann, P., and Güntherodt, H.-J. (1994) Tip artefacts in scanning force microscopy. *J. Microsc.* **173,** 183–197.
28. Kimura, Y., Vassylyev, D. G., Miyazawa, A., Kidera, A., Matsushima, M., Mitsuoka, K., Murata, K., et al. (1997) Surface of bacteriorhodopsin revealed by high-resolution electron crystallography. *Nature* **389,** 206–211.